Nanofriction in Cavity Quantum Electrodynamics

T. Fogarty,[1] C. Cormick,[2] H. Landa,[3] Vladimir M. Stojanović,[4] E. Demler,[4] and Giovanna Morigi[1]
[1]Theoretische Physik, Universität des Saarlandes, D-66123 Saarbrücken, Germany
[2]IFEG, CONICET and Universidad Nacional de Córdoba, Ciudad Universitaria, X5016LAE Córdoba, Argentina
[3]LPTMS, CNRS, Univ. Paris-Sud, Université Paris-Saclay, 91405 Orsay, France
[4]Department of Physics, Harvard University, Cambridge, Massachusetts 02138, USA
(Received 2 April 2015; published 1 December 2015)

The dynamics of cold trapped ions in a high-finesse resonator results from the interplay between the long-range Coulomb repulsion and the cavity-induced interactions. The latter are due to multiple scatterings of laser photons inside the cavity and become relevant when the laser pump is sufficiently strong to overcome photon decay. We study the stationary states of ions coupled with a mode of a standing-wave cavity as a function of the cavity and laser parameters, when the typical length scales of the two self-organizing processes, Coulomb crystallization and photon-mediated interactions, are incommensurate. The dynamics are frustrated and in specific limiting cases can be cast in terms of the Frenkel-Kontorova model, which reproduces features of friction in one dimension. We numerically recover the sliding and pinned phases. For strong cavity nonlinearities, they are in general separated by bistable regions where superlubric and stick-slip dynamics coexist. The cavity, moreover, acts as a thermal reservoir and can cool the chain vibrations to temperatures controlled by the cavity parameters and by the ions' phase. These features are imprinted in the radiation emitted by the cavity, which is readily measurable in state-of-the-art setups of cavity quantum electrodynamics.

DOI: 10.1103/PhysRevLett.115.233602 PACS numbers: 42.50.Ct, 37.10.Jk, 42.50.Pq, 63.70.+h

Cavity quantum electrodynamics (CQED) with cold atomic ensembles provides exciting settings in which to study the physics of long-range interacting systems [1,2]. The latter are found when the interparticle potential in D dimensions exhibits a scaling with the distance r slower than $1/r^D$ [3]. This property is of relevance from the nuclear scale to astrophysical plasmas and leads to nonadditivity of the energy, whose consequences are, among others, ensemble inequivalence and metastable states with diverging lifetimes [3].

The dynamics of atoms in single-mode high-finesse resonators exhibits several analogies with well-known theoretical models of the statistical mechanics of long-range interacting systems [4]. High-finesse cavities, in fact, trap photons for a sufficiently long time such that multiple scatterings can occur among the atoms inside the resonator. This gives rise to an effective interatomic potential whose range can scale with the size of the system [5] and that can induce spontaneous atom ordering [6,7] even in one dimension [8]. Additionally, the system is intrinsically out of equilibrium because the resonator dissipates light; thus, nontrivial phases are observed only in the presence of an external drive. Under these premises, photon shot noise gives rise to global retardation effects, which can effectively cool the atomic motion [1,4,8].

The interparticle forces in general compete with these dynamics. When the interactions are short ranged, at ultralow temperatures their interplay with the cavity potential can give rise to exotic phases, which tend to maximize photon scattering into the resonator and, thus, the strength of the long-range intracavity potential [1,7,9–11]. To a large extent, however, it is unknown how these dynamics are modified as the range of the competing interacting potential is increased. This question acquires further relevance in view of experimental setups trapping cold ions within high-finesse cavities [12–18].

In this Letter we theoretically characterize the effect of cavity backaction in the presence of the competing Coulomb interaction between N ions with the same charge q and mass m. The ions are confined by an external trap inside a standing-wave resonator of wavelength λ, in the geometry illustrated in Fig. 1(a), where their motion is assumed to be one dimensional along the x axis. This setup is expected to simulate the Frenkel-Kontorova model [19–21], which describes a chain of elastically bound particles subjected to an external periodic potential (substrate) in one dimension [12,13,22–25] and reproduces the salient features of stick-slip motion between two surfaces. When the periodicity $\lambda/2$ of the cavity optical lattice is incommensurate with the characteristic interparticle distance d of the ions (and the cavity nonlinearity is negligible), the ions' ground state can be either sliding or pinned: in the sliding phase the forces giving rise to sticking can cancel, so that the minimal force for initiating sliding vanishes. Static friction becomes significant when ions are pinned by the cavity potential; in this case, their distribution can still be incommensurate with the lattice periodicity, exhibiting defects (kinks). In the FK model the sliding and pinned phases are separated by the Aubry transition, whose control field is the relative amplitude of the periodic potential [26–28], and whose hallmark is the abrupt growth of the lowest phonon frequency (phonon gap) [29]. In a finite chain with free ends and an inversion-symmetric

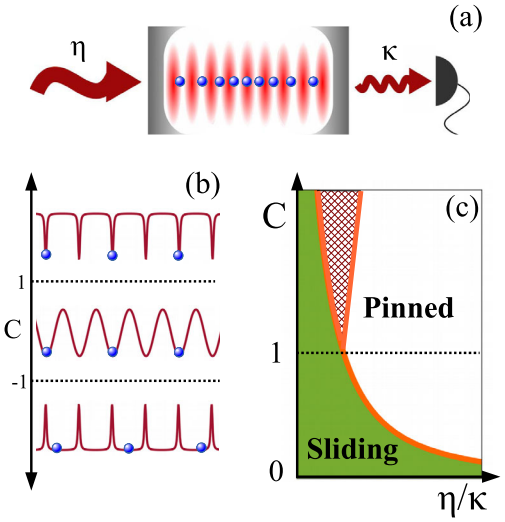

FIG. 1 (color online). (a) An array of cold ions in the optical lattice of a high-finesse cavity is an exotic realization of the Frenkel-Kontorova (FK) model. The cavity is pumped by a laser with amplitude η and decays at rate κ, and the intracavity photon number is determined by the ion density; this gives rise to a globally deformable potential which depends nonlinearly on the ions' positions. (b) The functional form of the cavity-induced potential for one particle. In the pinned phase, the shape is approximately sinusoidal for $|C| < 1$, and for $|C| > 1$ it becomes flat everywhere except in the vicinity of minima ($C > 0$) or maxima ($C < 0$). (c) Sketch of the phase diagram for the stationary state as a function of η and of the cavity nonlinearity C (cooperativity). Typically for $|C| > 1$ bistable phases can be observed (shown by the hatched region), signifying that superlubric or stick-slip dynamics are found depending on the variation of η with time.

potential, this transition is characterized by symmetry breaking [21,28].

This behavior is substantially modified when the periodic potential of the resonator mediates a long-range interaction among the atoms in the dispersive regime of CQED [1,30]. Here, the coupling at strength g to a cavity field mode, with spatial mode function $\cos(kx)$ and $k=2\pi/\lambda$, induces the conservative potential $\hbar U_0 \hat{n} \cos^2(kx)$ for sufficiently large detuning $\Delta_0 = \omega_c - \omega_{\rm el}$ between the frequencies of the cavity mode and ion dipolar transition. Then, the potential amplitude is proportional to the intracavity photon number operator $\hat{n}$. The strong-coupling regime of CQED is reached when the dynamical Stark shift per atom $U_0 = g^2/\Delta_0$ is such that $N|U_0|/\kappa > 1$, with κ the cavity loss rate [1,30]. In this regime, the mean intracavity photon number $\bar{n} = \langle \hat{n} \rangle$; thus, the depth of the cavity optical lattice is a nonlinear function of the ions positions [31],

$$\bar{n} = |\eta|^2/[\kappa^2 + \Delta_{\rm eff}(\{x_j\})^2], \tag{1}$$

where η is the amplitude of the driving field and

$$\Delta_{\rm eff}(\{x_j\}) = \Delta_c - NU_0 B_N(\{x_j\}). \tag{2}$$

The detuning $\Delta_c = \omega_p - \omega_c$ of the pump from the cavity frequency is thus shifted by $NU_0 B_N(\{x_j\})$, where the function $B_N = \sum_j \cos^2(kx_j)/N$ depends on the ions' positions x_j along the cavity axis and is the so-called bunching parameter, as it measures their localization at the potential minima. This frequency shift is at the origin of the nonlinear dependence of $\bar{n}$ on $\{x_j\}$ and gives rise to a deformation of the effective potential that the ions experience, as shown in Fig. 1(b), which can be expressed in terms of the effective mean-field potential

$$V_{\rm cav} = -(\hbar|\eta|^2/\kappa) \arctan[\Delta_{\rm eff}(\{x_j\})/\kappa], \tag{3}$$

and whose derivation is reported in Refs. [31,32]. Its functional dependence is reminiscent of the nonlinearly deformable potential discussed in Refs. [33,34]. Potential $V_{\rm cav}$, however, also mediates a multibody long-range interaction between the ions and thus acts as a globally deformable potential, since the potential depth depends on the global variable B_N. It competes with the potential $V_{\rm ion}$ due to the Coulomb repulsion within the external harmonic trap, which orders the ions along the x axis [35,36], and whose axial component reads

$$V_{\rm ion} = \frac{1}{2}\sum_{j=1}^{N} m\omega^2 x_i^2 + \frac{q^2}{4\pi\epsilon_0}\sum_{j>i}\frac{1}{|x_j - x_i|}, \tag{4}$$

with ω the trap frequency along x. In the absence of the cavity, the equilibrium positions $\{x_i^{(0)}\}$ form a chain; the interparticle distance $d_j = x_{j+1}^{(0)} - x_j^{(0)}$ is inhomogeneous but almost uniform at the chain center [37], where it takes the minimal value d. Within the resonator the ions' equilibrium positions $\{\bar{x}_j\}$ are the minima of the total potential $V = V_{\rm ion} + V_{\rm cav}$. We choose the trap frequency ω to ensure an incommensurate ratio between λ and d, such that the dynamics are intrinsically frustrated.

The strength of the cavity-mediated interactions is controlled by the cooperativity $C = NU_0/\kappa$, which scales the strength of the nonlinear shift in Eq. (2). For $|C| \ll 1$ the mean photon number is independent of the ions' positions. In this limit $V_{\rm cav} \approx V_0 \sum_j \cos^2(kx_j)$ and the total potential V can be mapped to the FK model [13,22,23]. The sliding-to-pinned transition is then expected at a critical value of the potential amplitude $V_0^c \propto \eta^2 C$, and occurs at smaller values of η with increasing $|C|$, as illustrated in Fig. 1(c). The sign of U_0, and thus of C, determines the features of the pinned phase: for $C > 0$, a pinned configuration minimizes B_N, since the minima of $V_{\rm cav}$ are at the nodes, while for $C < 0$ it maximizes B_N. As $|C|$ increases, the cavity potential changes shape, as in Fig. 1(b), and it strongly depends on the value of B_N through the shift in Eq. (2): for a fixed detuning Δ_c, the resonance $\Delta_{\rm eff} = 0$ is fulfilled for certain values of B_N, and thus for specific phases. For $|\Delta_c| > \kappa$, the resonance can directly separate the regime where the minima are either spikes or flat bottomed.

In order to evaluate the ions' phase we define an appropriate thermodynamic limit: since $C \propto N$, we scale $U_0 \sim 1/N$ to ensure that the resonance is at the same value of B_N [38]. To fix the ratio d/λ, the trap frequency is scaled as $\omega \sim \sqrt{\log(N)}/N$ [36]. The equilibrium positions of the ions in the total potential are numerically determined as a function of η, C, and Δ_c, and their stability is checked by means of a linear stability analysis. We characterize the stationary state by determining the corresponding bunching parameter and by classifying it in terms of a sliding or pinned phase. For this purpose, we compare the minimum phonon frequency [22,23] and an analog of the depinning force in the classical FK model [13,23,24], which is evaluated following the procedure discussed in Ref. [24,32]. For $C > 0$, for instance, the trap center ($x = 0$) is at a maximum, so for an odd number of ions, the sliding-to-pinned transition can be observed through the sudden displacement of the central ion from the origin. For larger C a finite force is required to restore the symmetry of the system. At this transition we verify that the phonon gap is zero, and in the pinned regime it increases monotonically. Analogous considerations apply for $C < 0$, where the maxima of the potential are at the antinodes of the field (in this case the center of the trap is shifted by $\lambda/4$ to obtain a symmetry breaking). We check that the values of η and C found by the symmetry-breaking transition are the same at which the phonon gap starts to increase [32].

The resulting phase diagram is shown in Figs. 2(a) and 2(b) for 11 ions and as a function of η and C for $\Delta_c = 0$ and $\Delta_c = -2\kappa$, respectively, using the parameters of Ref. [12]. It exhibits sliding (S), pinned (P), and bistable phases (hatched). The color code gives the corresponding value of B_N. We have checked that the diagram remains substantially unvaried as the number of ions is scaled up according to the thermodynamic limit, apart from the bistable phases at $C > 0$, as we discuss below. We first consider the transition line, delimiting the S phase. This moves to smaller values of η as $|C|$ increases. For $|C| < 1$, the backaction due to the resonator can be neglected and the line follows the expected behavior for the FK limit, with $\eta = \eta_c \sim 1/\sqrt{|C|}$. Here, it separates the S from the P phase and exhibits the typical features of the Aubry transition. At larger values it changes functional dependence. Moreover, sliding and pinned phases can coexist for $|C| > 1$ about the transition line, a typical feature of a first-order transition.

The bistable areas at $C > 0$, however, are of different nature than the ones for $C < 0$. For $C > 0$ they are due to finite-size effects. As C increases, in fact, the effective cavity potential becomes flat except for the nodes, where it exhibits tight minima, see Fig. 1(b). Thus, this potential supports a stable sliding phase that is symmetric about the center, where the ions in general experience a flat potential. As N is varied, bistability is still observed, but it qualitatively changes its features. The bistable region in Fig. 2(b) for $C < 0$ is instead due to the resonance $\Delta_{\text{eff}} = 0$, and remains unvaried as N is scaled up according to our prescription. This resonance occurs for specific values of B_N, and thus for specific sets of $\{\bar{x}_j\}$. Analogous resonances have been reported in experiments with cold atoms in resonators [39–41] and in theoretical works on similar setups [9,31,42]. In our case the bistability indicates that either superlubric or stick-slip behaviors can be encountered depending on how the intensity η is varied in time. Figure 2(c) shows the phase diagram for $C = -2$ and as a function of η and Δ_c. For this parameter choice, the resonance $\Delta_{\text{eff}} = 0$ exists only for $\Delta_c < 0$, with values varying between the minimum and the maximum value of $-2B_N\kappa$, and is thus dependent on the bunching parameter.

The bunching parameter is a particularly relevant quantity, since its value can be extracted from the intensity of the

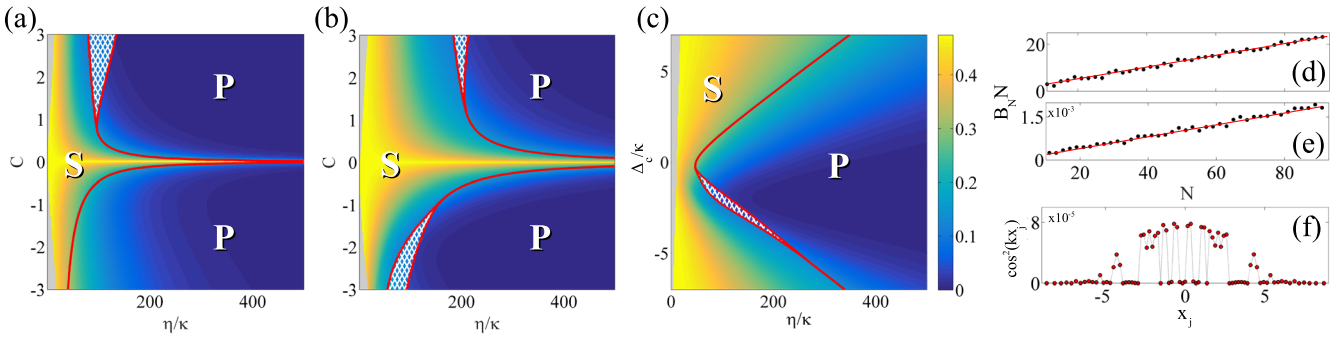

FIG. 2 (color online). Phase diagram as a function of C and η for (a) $\Delta_c = 0$, (b) $\Delta_c = -2\kappa$. In (c) the phase diagram is plotted as a function of Δ_c and η for cooperativity $C = -2$. Parameters η and Δ_c are in units of κ. The solid red line indicates the symmetry-breaking transition from the sliding (S) to the pinned (P) phase, and the hatched white region is an area of bistability. The color code gives the value of B_N for $C > 0$, and of $1 - B_N$ when $C < 0$. Subplots (d) and (e) display $B_N N$ vs N for $C = 0.5$, $\Delta_c = 0$, where (d) $\eta = 50\kappa$ and (e) $\eta = 500\kappa$, respectively. (f) The individual contributions $\cos^2(kx_j)$ to B_N for $N = 81$ particles, deep in the pinned phase ($B_N = 1.5 \times 10^{-3}$) for $C = 0.5$. The ions are $^{174}Yb^+$ and the parameters are $|\Delta_0| = 2\pi \times 12$ GHz and $\kappa = 2\pi \times 0.2$ MHz; for $N = 11$ the trap frequency is $\omega = 2\pi \times 1.12$ MHz, while g is varied in order to sweep over different values of C. The cavity wavelength is $\lambda = 369$ nm and the ratio $2d/\lambda = 7.3507$. The center of the harmonic trap corresponds with a maximum of V_{cav}, ensuring a symmetry-breaking transition. The grey area in (a)–(c) indicates where the mean phonon number $\bar{n} < 1$; outside of this region, our semiclassical analysis is reliable.

light at the cavity output. In the sliding phase and for $N \gg 1$, the particles are positioned at every point (modulus λ) of the cavity potential, and thus $\lim_{N\to\infty} B_N = 0.5$. In a commensurate phase, $B_N \to 0$ for $C > 0$ ($B_N \to 1$ for $C < 0$). At small deviations from this limiting value, B_N is a crude estimation of the kink density. The plots in Figs. 2(a) and 2(b) show that B_N signals the transition from sliding to pinned when $|C| \lesssim 0.5$; however, this is not the case for larger C. In general, therefore, for $B_N \sim 0.5$ the phase is sliding, while for $B_N < 0.05$ at $C > 0$ ($1 - B_N < 0.05$ at $C < 0$) the phase is tightly pinned. The estimated kink number $N_k \sim B_N N$ grows linearly with N, as shown in Figs. 2(d)–2(e): the slope decreases as η and C are increased but never vanishes, thus showing that the pinned phase remains incommensurate. Nonetheless, deep in the pinned phase the ions at the chain edges (where the density is smaller) organize at commensurate distances with λ, as depicted in Fig. 2(f). This effect results from the choice of harmonic confinement, and it shows that the edge ions enforce a boundary condition restricting the central ones from becoming truly commensurate.

Additional features of the cavity long-range interaction manifest in the ions' vibrations; they give rise to fluctuations in the potential, which in turn affects the ions' motion. We analyze the fluctuations in the linear regime and we denote $\delta\hat{a}$ and $\delta\hat{x}_j$ as the quantum fluctuations of the cavity annihilation operator and of the ion positions about the mean values $\bar{a} = \sqrt{\bar{n}}$ and $\bar{x}_j$, respectively, where $\bar{n}$ is given in Eq. (1) and $\bar{x}_j$ are the minima of V. We decompose the ions' displacement $\delta\hat{x}_j$ in the normal modes $\hat{q}_n = (\hat{b}_n + \hat{b}_n^\dagger)/\sqrt{2}$ calculated at zero order in $\delta\hat{a}$, with $\hat{b}_n$ the bosonic operator annihilating a chain phonon at frequency ω_n. Cavity and phonons are coupled by the linearized Heisenberg-Langevin equations in the presence of noise due to both the cavity decay and due to an external damping reservoir coupled with the motion [31,32]

$$\delta\dot{\hat{a}} = (\mathrm{i}\Delta_{\mathrm{eff}} - \kappa)\delta\hat{a} - \mathrm{i}\bar{a}\sum_n c_n(\hat{b}_n + \hat{b}_n^\dagger) + \sqrt{2\kappa}\hat{a}_{\mathrm{in}}, \quad (5)$$

$$\dot{\hat{b}}_n = -(\mathrm{i}\omega_n + \Gamma_n)\hat{b}_n - \mathrm{i}\bar{a}c_n(\delta\hat{a} + \delta\hat{a}^\dagger) + \sqrt{2\Gamma_n}\hat{b}_{\mathrm{in},n}, \quad (6)$$

where c_n denotes the cavity coupling with mode n and Γ_n is the mode's damping rate. The Langevin operators $\hat{\zeta}_{\mathrm{in}} = \hat{a}_{\mathrm{in}}, \hat{b}_{\mathrm{in},n}$ have zero mean value and $\langle[\hat{\zeta}_{\mathrm{in}}(t'), \hat{\zeta}_{\mathrm{in}}^\dagger(t'')]\rangle = \delta(t' - t'')$. The solutions are stationary when the eigenvalues possess no positive real parts. For $\Gamma_n = 0$, the stability is determined by the cavity parameters and is warranted when $\Delta_{\mathrm{eff}} < 0$ [the stability diagrams for the plots in Figs. 2(a)–2(b) are in the Supplemental Material [32]]. In this regime, retardation processes in photon scattering cool the chain to effective temperatures T which depend on the detuning Δ_c and on the bunching parameter B_N. Thus, the ions stationary state determines the temperature at which the chain is cooled. In turn, for a given Δ_c disparate regions in Figs. 2(a)–2(c) are generally at different temperatures because B_N and C vary. From Eq. (2), one sees that for $\Delta_c < 0$ and $C > 0$ the ions are always cooled. Cooling for $C < 0$ is found by suitably modifying the cavity detuning. In order to estimate T, we cast the modes in the form of a covariance matrix: for the parameters of Ref. [13] and $N = 11$ ions, we find that $T \sim 125$ μK can be reached. In this limit, the standard deviation from the equilibrium positions, $\langle\delta\hat{x}_j^2\rangle^{1/2}$, is smaller than $\lambda/2$ in the pinned phase; thus, the classical equilibrium conditions dictate the phases of the system. This condition can be achieved for any point of the phase diagram, i.e., also for $\Delta_{\mathrm{eff}} > 0$, by sympathetically cooling the chain [43] corresponding to an external reservoir with $\Gamma_n > 0$ in Eqs. (5)–(6).

The spectrum of the field emitted by the cavity, $\hat{a}_{\mathrm{out}}$, contains information about the collective vibrational modes of the ions within the resonator [44,45]. The output field is formally connected to the cavity field via the relation $\hat{a}_{\mathrm{out}} = \hat{a}_{\mathrm{in}} + \sqrt{2\kappa}\hat{a}$ [46], and its power spectrum is given by $S(\nu) \propto \langle\hat{\tilde{a}}_{\mathrm{out}}(\nu)^\dagger\hat{\tilde{a}}_{\mathrm{out}}(\nu)\rangle$, where $\hat{\tilde{a}}_{\mathrm{out}}(\nu)$ is the Fourier transform of $\hat{a}_{\mathrm{out}}(t)$ [31,32]. Figure 3 displays $S(\nu)$ for parameters such that the ions phases are sliding [Fig. 3(a)] and pinned [Fig. 3(b)]. For each phase we took the same values of B_N but different values of C. The peaks correspond to vibrational modes coupled to the cavity, and it is apparent that in the pinned phase more peaks are visible. This is a result of the broken symmetry induced by the optical lattice potential. The effect of the cavity backaction is weak in the sliding phase; the only discernible change in the spectrum is its relative intensity. In the pinned phase, however, the intricacies of the backaction are particularly apparent. Here the spread of the cavity frequencies becomes more separated for $C = -2$ due to the softening of the cavity pinning [see Fig. 1(b)], resulting in the emergence of three distinct frequency bands. Contrary to this, when $C = -0.5$, the ions are tightly restricted to the potential minima resulting in a narrow frequency band.

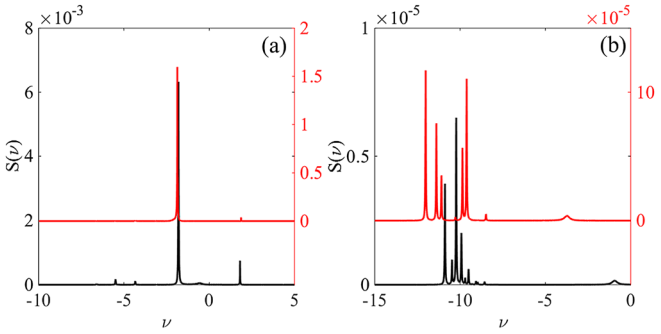

FIG. 3 (color online). Spectrum at the cavity output $S(\nu)$ (in arbitrary units) for $C < 0$ (a) in the sliding phase with $B_N = 1$–0.45 and (b) in the pinned phase with $B_N = 1$–0.05, for $C = -0.5$ (black line) and $C = -2$ (red line), and for 11 $^{174}\mathrm{Yb}^+$ ions, $\Delta_c = 0$, $\Gamma_n = 0.1\kappa$, and $T = 100$ μK. The resonances correspond to vibrational eigenmodes coupling with the cavity field and change in the pinned phase as C is increased. The elastic peak at ω_p (corresponding to $\nu = 0$) is not reported.

Our analysis is performed for parameters that are consistent with ongoing experiments, joining trapped ions and CQED setups [12–16] where the nonlinearity can be experimentally tuned by changing the number of atoms. This study is an example of competing long-range self-organization mechanisms which realizes a new paradigm of the Frenkel-Kontorova model. As well as displaying novel phases, such as bistability induced by the cavity-mediated interactions, the inherent losses from the cavity can cool the ions in a controlled manner and allow one to monitor the phases at the cavity output, thus setting the basis for feedback mechanisms controlling the thermodynamics of friction.

We thank M. Henkel, K. Rojan, and R. Bennewitz for discussions. Financial support from the German Research Foundation (DFG, DACH project "Quantum crystals of matter and light"), from the French government via the 2013–2014 Chateaubriand Fellowship, and from Harvard-MIT CUA, NSF Grant No. DMR-1308435, AFOSR Quantum Simulation MURI, the ARO-MURI on Atomtronics, and the ARO MURI Quism program, Dr. Max Rössler, the Walter Haefner Foundation and the ETH Foundation, is acknowledged. V. M. S. was supported by the SNSF.

[1] H. Ritsch, P. Domokos, F. Brennecke, and T. Esslinger, Cold atoms in cavity-generated dynamical optical potentials, Rev. Mod. Phys. **85**, 553 (2013).

[2] R. Bachelard, T. Manos, P. de Buyl, F. Staniscia, F. S. Cataliotti, G. De Ninno, D. Fanelli, and N. Piovella, Experimental perspectives for systems based on long-range interactions, J. Stat. Mech. (2010) P06009.

[3] A. Campa, T. Dauxois, and S. Ruffo, Statistical mechanics and dynamics of solvable models with long-range interactions, Phys. Rep. **480**, 57 (2009).

[4] S. Schütz and G. Morigi, Prethermalization of Atoms due to Photon-Mediated Long-Range Interactions, Phys. Rev. Lett. **113**, 203002 (2014).

[5] P. Münstermann, T. Fischer, P. Maunz, P. W. H. Pinkse, and G. Rempe, Observation of Cavity-Mediated Long-Range Light Forces between Strongly Coupled Atoms, Phys. Rev. Lett. **84**, 4068 (2000).

[6] A. T. Black, H. W. Chan, and V. Vuletić, Observation of Collective Friction Forces Due to Spatial Self-Organization of Atoms: From Rayleigh to Bragg Scattering, Phys. Rev. Lett. **91**, 203001 (2003).

[7] K. Baumann, C. Guerlin, F. Brennecke, and T. Esslinger, Dicke quantum phase transition with a superfluid gas in an optical cavity, Nature (London) **464**, 1301 (2010).

[8] P. Domokos and H. Ritsch, Collective Cooling and Self-Organization of Atoms in a Cavity, Phys. Rev. Lett. **89**, 253003 (2002).

[9] J. Larson, B. Damski, G. Morigi, and M. Lewenstein, Mott-Insulator States of Ultracold Atoms in Optical Resonators, Phys. Rev. Lett. **100**, 050401 (2008).

[10] S. Gopalakrishnan, B. L. Lev, and P. M. Goldbart, Emergent crystallinity and frustration with Bose-Einstein condensates in multimode cavities, Nat. Phys. **5**, 845 (2009).

[11] H. Habibian, A. Winter, S. Paganelli, H. Rieger, and G. Morigi, Bose-Glass Phases of Ultracold Atoms Due to Cavity Backaction, Phys. Rev. Lett. **110**, 075304 (2013).

[12] M. Cetina, A. Bylinskii, L. Karpa, D. Gangloff, K. M. Beck, Y. Ge, M. Scholz, A. T. Grier, I. Chuang, and V. Vuletić, One-dimensional array of ion chains coupled to an optical cavity, New J. Phys. **15**, 053001 (2013).

[13] A. Bylinskii, D. Gangloff, and V. Vuletić, Tuning friction atom-by-atom in an ion-crystal simulator, Science **348**, 1115 (2015).

[14] R. B. Linnet, I. D. Leroux, M. Marciante, A. Dantan, and M. Drewsen, Pinning an Ion with an Intracavity Optical Lattice, Phys. Rev. Lett. **109**, 233005 (2012).

[15] B. Casabone, K. Friebe, B. Brandstätter, K. Schüppert, R. Blatt, and T. E. Northup, Enhanced Quantum Interface with Collective Ion-Cavity Coupling, Phys. Rev. Lett. **114**, 023602 (2015).

[16] B. Casabone, A. Stute, K. Friebe, B. Brandstätter, K. Schüppert, R. Blatt, and T. E. Northup, Heralded Entanglement of Two Ions in an Optical Cavity, Phys. Rev. Lett. **111**, 100505 (2013).

[17] L. Lamata, D. R. Leibrandt, I. L. Chuang, J. I. Cirac, M. D. Lukin, V. Vuletić, and S. F. Yelin, Ion Crystal Transducer for Strong Coupling Between Single Ions and Single Photons, Phys. Rev. Lett. **107**, 030501 (2011).

[18] A. Stute, B. Casabone, P. Schindler, T. Monz, P. O. Schmidt, B. Brandstätter, T. E. Northup, and R. Blatt, Tunable ion-photon entanglement in an optical cavity, Nature (London) **485**, 482 (2012).

[19] O. M. Braun and Yu. S. Kivshar, *The Frenkel-Kontorova Model: Concepts, Methods, and Applications* (Springer, New York, 2004).

[20] Ya. I. Frenkel and T. A. Kontorova, The model of dislocation in solid body, Zh. Eksp. Teor. Fiz. **8**, 1340 (1938) [Phys. Z. Sowjetunion **13**, 1 (1938)].

[21] O. Biham and D. Mukamel, Global universality in the Frenkel-Kontorova model, Phys. Rev. A **39**, 5326 (1989).

[22] I. García-Mata, O. V. Zhirov, and D. L. Shepelyansky, Frenkel-Kontorova model with cold trapped ions, Eur. Phys. J. D **41**, 325 (2007).

[23] T. Pruttivarasin, M. Ramm, I. Talukdar, A. Kreuter, and H. Häffner, Trapped ions in optical lattices for probing oscillator chain models, New J. Phys. **13**, 075012 (2011).

[24] A. Benassi, A. Vanossi, and E. Tosatti, Nanofriction in cold ion traps, Nat. Commun. **2**, 236 (2011).

[25] D. Mandelli, A. Vanossi, and E. Tosatti, Stick-slip nanofriction in trapped cold ion chains, Phys. Rev. B **87**, 195418 (2013).

[26] S. Aubry, The twist map, the extended Frenkel-Kontorova model and the devil's staircase, Physica (Amsterdam) **7D**, 240 (1983); S. Aubry and P. Y. Le Daeron, The discrete Frenkel-Kontorova model and its extensions, Physica (Amsterdam) **8D**, 381 (1983).

[27] S. R. Sharma, B. Bergersen, and B. Joos, Aubry transition in a finite modulated chain, Phys. Rev. B **29**, 6335 (1984).

[28] Y. Braiman, J. Baumgarten, J. Jortner, and J. Klafter, Symmetry-Breaking Transition in Finite Frenkel-Kontorova Chains, Phys. Rev. Lett. **65**, 2398 (1990).

[29] M. Peyrard and S. Aubry, Critical behavior at the transition by breaking of analyticity in the discrete Frenkel-Kontorova model, J. Phys. C **16**, 1593 (1983).

[30] H. J. Kimble, in *Cavity Quantum Electrodynamics*, edited by P. R. Berman (Academic Press, New York, 1994), p. 203.

[31] C. Cormick and G. Morigi, Structural Transitions of Ion Strings in Quantum Potentials, Phys. Rev. Lett. **109**, 053003 (2012); Ion chains in high-finesse cavities, Phys. Rev. A **87**, 013829 (2013).

[32] See Supplemental Material at http://link.aps.org/supplemental/10.1103/PhysRevLett.115.233602 for topics related to the modelling and numerics of this Letter.

[33] M. Peyrard and M. Remoissenet, Solitonlike excitations in a one-dimensional atomic chain with a nonlinear deformable substrate potential, Phys. Rev. B **26**, 2886 (1982).

[34] J. Tekić, P. Mali, Z. Ivić, and M. Pantić, Size effect of the subharmonic Shapiro steps on the interference phenomena in the Frenkel-Kontorova model with realistic substrate potentials, J. Appl. Phys. **114**, 174504 (2013).

[35] D. H. E. Dubin and T. M. O'Neil, Trapped nonneutral plasmas, liquids, and crystals (the thermal equilibrium states), Rev. Mod. Phys. **71**, 87 (1999).

[36] G. Morigi and S. Fishman, Dynamics of an ion chain in a harmonic potential, Phys. Rev. E **70**, 066141 (2004).

[37] D. H. E. Dubin, Minimum energy state of the one-dimensional Coulomb chain, Phys. Rev. E **55**, 4017 (1997).

[38] S. Fernandez-Vidal, G. De Chiara, J. Larson, and G. Morigi, Quantum ground state of self-organized atomic crystals in optical resonators, Phys. Rev. A **81**, 043407 (2010).

[39] B. Nagorny, Th. Elsässer, and A. Hemmerich, Collective Atomic Motion in an Optical Lattice Formed Inside a High Finesse Cavity, Phys. Rev. Lett. **91**, 153003 (2003); Th. Elsässer, B. Nagorny, and A. Hemmerich, Optical bistability and collective behavior of atoms trapped in a high-Q ring cavity, Phys. Rev. A **69**, 033403 (2004).

[40] S. Gupta, K. L. Moore, K. W. Murch, and D. M. Stamper-Kurn, Cavity Nonlinear Optics at Low Photon Numbers from Collective Atomic Motion, Phys. Rev. Lett. **99**, 213601 (2007); T. P. Purdy, D. W. C. Brooks, T. Botter, N. Brahms, Z.-Y. Ma, and D. M. Stamper-Kurn, Tunable Cavity Optomechanics with Ultracold Atoms, *ibid.* **105**, 133602 (2010).

[41] F. Brennecke, S. Ritter, T. Donner, and T. Esslinger, Cavity optomechanics with a Bose-Einstein condensate, Science **322**, 235 (2008); S. Ritter, F. Brennecke, K. Baumann, T. Donner, C. Guerlin, and T. Esslinger, Dynamical coupling between a Bose-Einstein condensate and a cavity optical lattice, Appl. Phys. B **95**, 213 (2009).

[42] W. Chen, K. Zhang, D. S. Goldbaum, M. Bhattacharya, and P. Meystre, Bistable Mott-insulator-to-superfluid phase transition in cavity optomechanics, Phys. Rev. A **80**, 011801(R) (2009).

[43] D. J. Wineland, C. Monroe, W. M. Itano, D. Leibfried, B. E. King, and D. M. Meekhof, Resolved-sideband Raman cooling of a bound atom to the 3D zero-point energy, J. Res. Natl. Inst. Stand. Technol. **103**, 259 (1998).

[44] A. Dantan, J. P. Marler, M. Albert, D. Guot, and M. Drewsen, Noninvasive Vibrational Mode Spectroscopy of Ion Coulomb Crystals Through Resonant Collective Coupling to an Optical Cavity Field, Phys. Rev. Lett. **105**, 103001 (2010).

[45] N. Brahms, T. Botter, S. Schreppler, D. W. C. Brooks, and D. M. Stamper-Kurn, Optical Detection of the Quantization of Collective Atomic Motion, Phys. Rev. Lett. **108**, 133601 (2012).

[46] C. W. Gardiner and M. J. Collett, Input and output in damped quantum systems: Quantum stochastic differential equations and the master equation, Phys. Rev. A **31**, 3761 (1985).